Diversity of Dynamics and Morphologies of Invasive Solid Tumors

Yang Jiao*

Physical Science in Oncology Center,

Princeton University, Princeton New Jersey 08544, USA

Salvatore Torquato†

Department of Chemistry, Princeton University,

Princeton New Jersey 08544, USA

Department of Physics, Princeton University,

Princeton New Jersey 08544, USA

Physical Science in Oncology Center,

Princeton University, Princeton New Jersey 08544, USA

Princeton Center for Theoretical Science,

Princeton University, Princeton New Jersey 08544, USA and

Program in Applied and Computational Mathematics,

Princeton University, Princeton New Jersey 08544, USA

(Dated: January 5, 2012)

Abstract

Complex tumor-host interactions can significantly affect the growth dynamics and morphologies of progressing neoplasms. The growth of a confined solid tumor induces mechanical pressure and deformation of the surrounding microenvironment, which in turn influences tumor growth. In this paper, we generalize a recently developed cellular automaton model for invasive tumor growth in heterogeneous microenvironments [Y. Jiao and S. Torquato, *PLoS Comput. Biol.* **7**, e1002314 (2011)] by incorporating the effects of pressure. Specifically, we explicitly model the pressure exerted on the growing tumor due to the deformation of the microenvironment and its effect on the local tumor-host interface instability. Both *noninvasive-proliferative* growth and *invasive* growth with individual cells that detach themselves from the primary tumor and migrate into the surrounding microenvironment are investigated. We find that while *noninvasive* tumors growing in "soft" homogeneous microenvironments develop almost isotropic shapes, both high pressure and host heterogeneity can strongly enhance malignant behavior, leading to finger-like protrusions of the tumor surface. Moreover, we show that individual invasive cells of an *invasive* tumor degrade the local extracellular matrix at the tumor-host interface, which diminishes the fingering growth of the primary tumor. The implications of our results for cancer diagnosis, prognosis and therapy are discussed.

PACS numbers: 87.19.lx, 46.32.+x, 87.17.Pq

I. INTRODUCTION

Tumor malignancy arises from many complex interactions occurring between the tumor and its host microenvironment.[1,2] There is increasing evidence that the host microenvironment can significantly affect neoplasm progression.[3–20] The growth of a confined solid tumor also produces mechanical pressure, leading to deformation of the surrounding microenvironment, which generally affects the growth dynamics of the tumor.[21] Such pressure can result in clinical complications, especially in a confined region of space such as the brain[22] and deform or even collapse the intra-tumoral blood and lymphatic vessels.[23] It has been hypothesized that pressure may also influence tumor physiology, growth rate and morphology.[21] Therefore, understanding effects of pressure on tumor growth is important for both fundamental cancer research and clinical practice.[21]

Mechanical interactions between a tumor and its microenvironment is a topic of great interest. In the work of Helmlinger et al,[21] it was shown that pressure can significantly reduce tumor growth rate and even inhibit tumor growth *in vivo*. Bru and Casero[24] studied the effect of external pressure on the growth of tumor cell colonies and showed that tumor morphology strongly depends on the pressure exerted by the surrounding medium. Moreover, it has been observed that stiffer microenvironments can promote malignant behavior.[25] For example, tumors embedded in low-density soft agarose gels remain roughly spherical in shape; however, they could exhibit a finger-like morphology in a stiff gel with high density.[26]

A variety of analytical and computational models have been developed to incorporate the effect of pressure on tumor growth. In particular, McElwain and Pettet[27] considered that tumor cells mechanically behave as incompressible "bags" of fluid enclosed by the plasma membrane. Chen et al.[28] modeled the growth of tumor spheroids in agarose gels, considering the agarose gel to be a elastic material undergoing large deformations and the tumor tissue was approximated by a fluid-like material with additional drag and surface tension effects. Roose et al.[29] employed a linear poroelasticity model to estimate the solid stress generated by the growth of the tumor spheroid. Although the overall growth of the tumor spheroid can be well described by these analytical approaches, they are not able to provide detailed information on the tumor morphology. Gevertz et al.[7,8] employed a cellular automaton model to investigate the effects the shape of an organ on growing tumors through mechanical interactions. Using coupled nonlinear partial differential equations, Macklin and Lowengrub[19]

modeled the response of the tissue surrounding the tumor to the proliferation-induced mechanical pressure. Specifically, these authors found that tumors growing in mechanically unresponsive (i.e., rigid) microenvironments develop invasive fingering morphologies and tumors growing in mechanically responsive (i.e., soft) microenvironment develop compact morphologies. However, since a continuum method is used, it is not possible to keep track of individual invasive cells that detach themselves from the primary tumor and how such invasive cells affect the growth dynamics and morphologies of the primary tumor.

Recently, we presented a single-cell based cellular automaton (CA) model for invasive tumor growth in heterogeneous microenvironments[30] in response to the challenge of developing an "Ising" model for cancer growth.[31] In this CA model, individual invasive cells can detach themselves from the primary tumor, locally degrade the extracellular matrix (ECM) and invade into the surrounding host microenvironment. A rich spectrum of emergent properties and coupled growth dynamics of the primary tumor and invasive cells were predicted. However, the effects of pressure exerted by the outer boundary of the growth permitting region (e.g., cranium) on the tumor and the deformation of the ECM were only implicitly considered.

In this paper, we generalize the aforementioned CA model to explicitly take into account the deformation of the ECM surrounding an invasive or noninvasive tumor, which in turn imposes pressure on the neoplasm. Moreover, we also explicitly consider the local geometry of the tumor-host interface (i.e., the tumor surface), which can either enhance or reduce local growth (i.e., interface instability) depending on the local curvature of the interface. Both *noninvasive-proliferative* growth and *invasive* growth with individual cells that detach themselves from the primary tumor and migrate into the surrounding microenvironment are investigated. We show here that by varying the ECM rigidity (density), one can obtain a continuous spectrum of tumor morphologies ranging from smooth isotropic shapes to fingering patterns, which have been observed both *in vitro* and *in vivo*[19]. The specific surface[32] is employed to quantify the degree of "fingering" for noninvasive proliferative growth. We find that both the high pressure built up due to tumor growth and the microenvironment heterogeneity can significantly promote malignancy of the noninvasive proliferative tumor. Moreover, we show that individual invasive cells that leave an invasive primary tumor degrade the local ECM at the tumor-host interface, which diminishes the fingering growth of the primary tumor. Our results concerning the diversity of tumor morphologies enable one

to infer what are the possible mechanisms behind the resulting shapes. Such information is expected to be of great value for cancer diagnosis, prognosis and therapy.

II. COMPUTATIONAL METHODS

Following Refs. [7,8,30,33–35], we use the Voronoi tessellation associated with random-sequential-addition (RSA) sphere packings[32] to model the underlying cellular structure. In particular, nonoverlapping d-dimensional spheres ($d = 2$ and 3) are randomly and sequentially placed in a prescribed region in d-dimensional Euclidean space until there is no void space left for additional spheres. Then, space is divided into polyhedra, each associated with a sphere center, such that any points within a polyhedron is closer to its associated sphere center than to any other sphere centers. The resulting Voronoi polyhedra are referred to as automaton cells, which can represent either real biological cells or regions of tumor stroma.

Here we explicitly takes into account the interactions between a single cell and the surrounding microenvironment. Thus, each automaton cell represents either a *single* tumor cell (approximately $15 - 20$ μm in size) or a region of tumor stroma of similar size. In the current model, we mainly focus on the effects of the ECM macromolecule density, ECM degradation by the malignant cells, and the pressure due to the ECM deformation on tumor growth. Henceforth, we will refer to the host microenvironment (or tumor stroma) as the "ECM" for simplicity. Each ECM associated automaton cell is assigned a particular density $\rho_{\rm ECM}$, representing the density of the ECM molecules within the automaton cell. A tumor cell can occupy an ECM associated automaton cell only if the density of this automaton cell $\rho_{\rm ECM} = 0$, which means that either the ECM is degraded or it is deformed (pushed away) by the proliferating tumor cells.

A. Modeling the Pressure Exerted on the Growing Tumor

The extracellular matrix is a complex mixture of macromolecules and interstitial fluids that provides mechanical supports for the tissue and plays an important role for cell adhesion and motility.[36] In general, the ECM can be highly heterogeneous, with large spatial variations of the ECM macromolecule densities $\rho_{\rm ECM}$. Our simulated tumors are only allowed to grow in a compact growth-permitting region in order to mimic the physical confinement of the

host microenvironment, such as the boundary of an organ or cranium in the case of the brain. Therefore, a growing tumor deforms the ECM, which in turn imposes a pressure on the tumor.[21,37,38]

In Ref. 30, we considered the effects of the local ECM density on the proliferating cells. In this work, the ECM with larger density was considered to be more rigid and more difficult to degrade/deform. Therefore, the probability of division p_{div}, which is related to the cell doubling time τ_0 by $\tau_0 = \ln 2/\ln(1 + p_{div})$, was taken to be a monotonically decreasing function of $\rho_{\rm ECM}$, e.g.,

$$p_{div} \sim (1 - \rho_{\rm ECM}). \tag{1}$$

The effect of pressure was only considered implicitly, e.g., $p_{div} \sim (1 - r/L_{max})$, where r is the distance of the dividing cell from the tumor centroid, L_{max} is the distance between the closest growth-permitting boundary cell in the direction of tumor growth and the tumor centroid.

Here we explicitly consider the pressure exerted on the growing tumor by the ECM due to deformation. In particular, we consider that the ECM is a linear elastic medium with bulk modulus $\kappa_{\rm ECM}$. The pressure P due to volume deformation ΔV is given by

$$P = \kappa_{\rm ECM}\frac{\Delta V}{V}, \tag{2}$$

where V is the initial volume of the ECM. The ECM density $\rho_{\rm ECM} = M/V$, where M is the ECM mass. Therefore, the ECM density increase due to small volume shrinkage, i.e.,

$$\rho_{\rm ECM} = M/(V - \Delta V) \approx (M/V)(1 + \Delta V) = \rho^0_{\rm ECM}(1 + \Delta V), \tag{3}$$

which gives

$$\frac{\Delta V}{V} = \frac{(\rho_{\rm ECM} - \rho^0_{\rm ECM})}{\rho^0_{\rm ECM}}. \tag{4}$$

Substituting Eq. (4) into Eq. (2), we have

$$P = \kappa_{\rm ECM}\frac{\Delta V}{V} = \kappa_{\rm ECM}\frac{(\rho_{\rm ECM} - \rho^0_{\rm ECM})}{\rho^0_{\rm ECM}}. \tag{5}$$

In other words, the pressure exerted by the ECM due to deformation is proportional to its density, i.e., $P \sim (\rho_{\rm ECM} - \rho^0_{\rm ECM})$. Without loss of generality, we consider that cell division probability is simply a monotonically decreasing function of pressure, and thus, also a monotonically decreasing function of the ECM density, i.e.,

$$p_{div} = (1 - \omega P) \sim \left[1 - \omega\frac{\kappa_{\rm ECM}}{\rho^0_{\rm ECM}}(\rho_{\rm ECM} - \rho^0_{\rm ECM})\right] = [1 - \frac{\omega^*}{\rho^0_{\rm ECM}}(\rho_{\rm ECM} - \rho^0_{\rm ECM})], \tag{6}$$

where

$$\omega^* = \omega\kappa_{\rm ECM} \tag{7}$$

is a constant of proportionality.

Suppose that the proliferative cells possess the ECM degradation ability χ_0, which is the fraction of the ECM macromolecules degraded by malignant cells per day per unit volume. After each day, the total mass of the ECM that has been degraded is

$$\Delta M = \chi_0 \sum_i^n \rho_{\rm ECM}(i) v(i), \tag{8}$$

where n is the total number of the ECM associated automaton cells taken by new tumor cells, $\rho_{\rm ECM}(i)$ and $v(i)$ are respectively the macromolecule density and volume associated with the ith automaton cell. The average ECM density is then given by

$$\rho_{\rm ECM} = \frac{M - \chi_0 \sum_i^n \rho_{\rm ECM}(i) v(i)}{V - \sum_i^n v(i)}. \tag{9}$$

We define the ratio of $\rho_{\rm ECM}/\rho^0_{\rm ECM}$ to be ξ, i.e.,

$$\xi = \frac{\rho_{\rm ECM}}{\rho^0_{\rm ECM}} = \frac{M - \chi_0 \sum_i^n \rho_{\rm ECM}(i) v(i)}{V - \sum_i^n v(i)} \frac{V}{M}. \tag{10}$$

The macromolecule densities of the remaining ECM automaton cells are then updated as

$$\rho_{\rm ECM}(j) = \xi \rho^0_{\rm ECM}(j), \tag{11}$$

i.e., the increase of the ECM density after deformation is proportional to its original density. Substitute Eq. (11) into Eq. (6), we have

$$p_{div} \sim \left[1 - \omega^*(\xi - 1)\right]. \tag{12}$$

We note that in the above analysis, we have neglected the deformation of the tumor cells, which possess a much larger bulk modulus $\kappa_{\rm cell}$ than that of the ECM, i.e., $\kappa_{\rm cell}/\kappa_{\rm ECM} \sim 100$ (see Ref. 29).

B. Modeling Local Tumor-Host Interface Instablity

Real tumors never possess a perfect spherical shape. Tumors growing even in a homogeneous soft ECM will develop a "bumpy" tumor surface, which can be very well captured by

our underlying cellular structure model (i.e., the Voronoi tessellation).[30] When growing in a rigid microenvironment, a locally smooth tumor surface which results in a huge pressure gradient at the surface is highly undesirable. On the other hand, locally small protrusions on the tumor surface can gain some growth advantage by further invading into the surrounding ECM to release local pressure.[26]

To model the aforementioned effects, we consider the local geometry of the protrusion tip. In particular, the width of the tip is taken to be the length w of the automaton cell at the tip. The length of the tip is given by

$$\ell = |\mathbf{x}_c - \overline{\mathbf{x}}|, \tag{13}$$

where $\mathbf{x}_c$ is the position of the center of the automaton cell at the tip and $\overline{\mathbf{x}} = \sum_i^m \mathbf{x}_i$ is the average center position of tumor cells neighboring the cell at the tip. The growth advantage of the cell at the tip is then proportional to ℓ/w, i.e.,

$$p_{div} \sim (1 + \ell/w). \tag{14}$$

We note that ℓ is effective the radius of curvature, which can be either positive or negative. A negative value of ℓ reduces p_{div}. For positive ℓ, the ratio ℓ/w is defined as the stress concentration factor associated with a crack tip in solid mechanics.

Other biophysical mechanisms associated with noninvasive and invasive malignant cells are the same as those described in Ref. 30. For example, the non-invasive cells remain in the primary tumor and can be proliferative, quiescent or necrotic, depending on their nutritional supply, which is determined by tumor-size dependent characteristic diffusion distances. Proliferative cells can produce "mutant" daughter cells that possess strong ECM degradation ability χ_1 and can leave the primary tumor and invade into the surrounding microenvironment by locally degrading the ECM macromolecules. Readers are referred to Ref. 30 for details of such mechanisms.

C. Cellular Automaton Rules

We now specify the CA rules for our generalized model, which closely follow those given in Ref. 30, except for the additional rules explicitly incorporating the pressure imposed by the ECM and the local host-tumor interface instability described here. After generating the

automaton cells using Voronoi tessellation, an ECM density $\rho_{\text{ECM}} \in (0,\ 1)$ is assigned to each automaton cell within the growth-permitting region, which represents the heterogeneous host microenvironment. Then a tumor is introduced by designating any one or more of the automaton cells as proliferative cancer cells. Time is then discretized into units that represent one real day. At each time step:

- Each automaton cell is checked for type: invasive, proliferative, quiescent, necrotic or ECM associated. Invasive cells degrade and migrate into the ECM surrounding the tumor. Proliferative cells are actively dividing cancer cells, quiescent cancer cells are those that are alive, but do not have enough oxygen and nutrients to support cellular division and necrotic cells are dead cancer cells.

- All tumorous necrotic cells are inert (i.e., they do not change type).

- Quiescent cells more than a certain distance δ_n from the tumor's edge are turned necrotic. The tumor's edge, which is assumed to be the source of oxygen and nutrients, consists of all ECM associated automaton cells that border the neoplasm. The critical distance δ_n for quiescent cells to turn necrotic is computed as follows:

$$\delta_n = aL_t^{(d-1)/d}, \tag{15}$$

  where a is a prescribed parameter (see Table I), d is the Euclidean spatial dimension and L_t is the distance between the geometric centroid $\mathbf{x}_c$ of the tumor and the tumor edge cell that is closest to the quiescent cell under consideration. The position of the tumor centroid $\mathbf{x}_c$ is given by

$$\mathbf{x}_c = \frac{\mathbf{x}_1 + \mathbf{x}_2 + \cdots + \mathbf{x}_N}{N}, \tag{16}$$

  where N is the total number of noninvasive cells contained in the tumor, which is updated when a new noninvasive daughter cell is added to the tumor.

- Each proliferative cell will attempt to divide with probability p_{div} into the surrounding ECM (i.e., the automaton cells associated with the ECM) by degrading and pushing away the ECM in that automaton cell. As discussed in the previous section, we consider that p_{div} for a specific proliferative cell depends on the local ECM density

[Eq. (1)], the pressure imposed by the ECM [Eq. (6)] and the local geometry of the tumor-host interface [Eq. (14)], i.e.,

$$p_{div} = \begin{cases} p_0[1 - \rho_{\text{ECM}} - \omega^*\xi & \text{if any ECM associated automaton cell within} \\ \quad +\omega^* + \xi\frac{\ell}{w}] & \text{the predefined growth distance is in the growth-} \\ & \text{permitting microenvironment} \\ & \\ & \text{if no ECM associated automaton cell within} \\ 0 & \text{the predefined growth distance is in the growth-} \\ & \text{permitting microenvironment, or the value} \\ & \text{of the above expression is negative} \end{cases} \tag{17}$$

where p_0 is the base probability of division (see Table I), r is the distance of the dividing cell from the tumor centroid, ρ_{ECM} is the ECM density of the automaton cell to be taken by the new tumor cell, ω^* and ξ are respectively given by Eq. (7) and Eq. (10). When a ECM associated automaton cell is taken by a tumor cell, its density is set to be zero. The predefined growth distance (δ_p) is described in the following bullet point.

- If a proliferative cell divides, it can produce a mutant daughter cell possessing an invasive phenotype with a prescribed probability γ (i.e., the mutation rate). The invasive daughter cell gains ECM degradation ability χ_1 and motility μ, which enables it to leave the primary tumor and invade into the surrounding ECM. The rules for updating invasive cells are given in the following bullet point. If the daughter cell is noninvasive, it is designated as a new proliferative cell.

- A proliferative cell turns quiescent if there is no space available for the placement of a daughter cell within a distance δ_p from the proliferative cell, which is given by

$$\delta_p = bL_t^{(d-1)/d},$$

where b is a nutritional parameter (see Table I), d is the spatial dimension and L_t is the distance between the geometric tumor centroid $\mathbf{x}_c$ and the tumor edge cell that is closest to the proliferative cell under consideration.

- An invasive cell degrades the surrounding ECM (i.e., those in the neighboring automaton cells of the invasive cell) and can move from one automaton cell to another if the

associated ECM is completely degraded locally. For an invasive cell with motility μ and ECM degradation ability χ_1, it will make m attempts to degrade the ECM in the neighboring automaton cells and jump to these automaton cells, where m is an arbitrary integer in $[0,\ \mu]$. For each attempt, the surrounding ECM density ρ_{ECM} is decreased by $\delta\rho$, where $\delta\rho$ is an arbitrary number in $[0,\ \chi_1]$. Using random numbers for the ECM degradation ability and cellular motility is to take into account tumor genome heterogeneity, which is manifested as heterogeneous phenotypes (such as different m and $\delta\rho$). When the ECM in multiple neighboring automaton cells of the invasive cell are completely degraded (i.e., $\rho_{\mathrm{ECM}} = 0$), the invasive cell moves in a direction that maximizes the nutrients and oxygen supply. Here we assume that the migrating invasive cells *do not divide*. The degraded ECM shows the invasive path of the tumor.

- The density ρ_{ECM} of the remaining ECM automaton cells is updated according to Eq. (11).

The important parameters mentioned in the bullet points above are summarized in Table I. We note that although only spherical growth-permitting regions are considered here, this constraint can be easily relaxed. As a demonstration of the capability and versatility of the generalized CA model, we will employ it to investigate the growth dynamics and morphologies of both noninvasive and invasive tumors in two dimensions. However, the model is easily extended to three dimensions and the algorithmic details of the model are presented for any spatial dimension.

III. RESULTS

Homogeneous and random distributions of the ECM density[30] are used to study the effects of microenvironment heterogeneity on the growing tumor. The random distribution of the ECM density, which henceforth is referred to as the "random ECM" for simplicity, is generated by assigning a random ECM density value between 0 and 1 to each ECM associated automaton cell. The boundary of the growth-permitting region is considered to be vascularized, i.e., a growing tumor can receive oxygen and nutrients from the growth-permitting region. In particular, we consider a constant radially symmetric nutrient/oxygen

TABLE I: Parameters and terms in the CA model. Summarized here are definitions of the parameters for tumor growth and invasion, and all other (time-dependent) quantities used in the simulations. The number(s) listed in parentheses indicates the value or range of values assigned to the corresponding parameters in the simulations. The values of the parameters are chosen such that the CA model can reproduce reported growth dynamics of GBM from the medical literature[3,7,33].

Time dependent terms	
L_t	Local tumor radius (varies with cell positions)
L_{max}	Local maximum tumor extent (varies with cell positions)
δ_p	Characteristic proliferative rim thickness
δ_n	Characteristic living-cell rim thickness (determines necrotic fraction)
p_{div}	Probability of division (varies with cell positions)
ρ_{ECM}	ECM density (depends on ECM deformation and varies with positions, > 0)
ξ	Ratio of current ECM density over initial density $\rho_{\mathrm{ECM}}/\rho^0_{\mathrm{ECM}}$
ω^*	Parameter measuring p_{div} reduced by pressure, $= 2\rho^0_{\mathrm{ECM}}$
Growth parameters	
p_0	Base probability of division, linked to cell-doubling time (0.192)
a	Base necrotic thickness, controlled by nutritional needs (0.58 $\mathrm{mm}^{1/2}$)
b	Base proliferative thickness, controlled by nutritional needs (0.30 $\mathrm{mm}^{1/2}$)
ℓ	Length of local protrusion tip
w	Width of local protrusion tip
χ_0	ECM degradation ability of proliferative cells ($0.0 - 0.25$)
Invasiveness parameters	
γ	Mutation rate (determines the number of invasive cells, 0.05)
χ_1	ECM degradation ability of invasive cells ($0.4 - 1.0$)
μ	Cell motility (the number of "jumps" from one automaton cell to another, $0 - 4$)

gradient in the growth-permitting region with the highest nutrient/oxygen concentration at the vascular boundary. We note that although generally the nutrient/oxygen concentration field *in vivo* is more complicated, previous numerical studies that considered the exact evolution of nutrient/oxygen concentrations have shown a decay of the concentrations toward the tumor center.[9,10] Since the directions of cell motions are determined by the nutrient/oxygen gradient only, our constant-gradient approximation is a very reasonable one.

In the beginning, a proliferative tumor cell is introduced at the center of the growth-permitting region and tumor growth is initiated. The parameters employed are either given in Table I or specified for each case separately. The specific surface s for the noninvasive proliferative tumor, defined as the ratio of the total length of the perimeter of the primary tumor over its total area,[30,32] is employed to quantify the degree of "fingering" of the growing tumor. For a perfectly circular shape with radius R, the associated s is given by $2/R$, which is the minimal value among all shapes with the same area. The specific surface of a tumor in excess of that of a circle provides a measurement of the roughness of the tumor surface and thus, the degree of "fingering". Therefore, the specific surface s scaled by $2/R_T$ associated with a circle is used for an arbitrary-shaped tumor with effective radius R_T (i.e., the average distance from tumor edge to tumor center). In the visualizations of the tumor that follow, we will use the following convention: The ECM degraded by the tumor cells is blue. In the primary tumor, necrotic cells are black, quiescent cells are yellow and proliferative cells are red. The invasive tumor cells are green.

A. Noninvasive Proliferative Growth

We first investigate the effects of pressure on the growth of noninvasive proliferative tumors by setting the mutation rate to zero, i.e., $\gamma = 0$. Figure 1 shows the snapshots of noninvasive tumors growing in the homogeneous ECM with initial density $\rho^0_{\rm ECM} = 0.25, 0.45$ and 0.65. The associated specific surface as a function of time is also shown. The ECM degradation ability value $\chi_0 = 0.2$ for the proliferative cells is used.

It can be clearly seen that as the ECM density (i.e., pressure level) varies, a variety of growth dynamics and tumor morphologies emerge. In particular, the tumor growing in the ECM with low density (pressure) ($\rho_{\rm ECM} = 0.25$) develops an almost isotropic shape with small specific surface $s/(2/R_T)$ (upper panel of Fig. 1). As the ECM density (pressure) increases

($\rho_{\rm ECM} = 0.45$), the tumor begins to develop bumpy surface, but a well-defined "spherical" core can still be identified (middle panel of Fig. 1). For the high ECM density (pressure) $\rho_{\rm ECM} = 0.65$, finger-like protrusions emerge at early growing stages and no "spherical" core of significant size is found (lower panel of Fig. 1). The associated specific surface $s/(2/R_T)$ monotonically increases as the tumor grows. Since the elongated finger-like structures of proliferative cells can grow into the nutrient-rich microenvironment, necrotic regions within these "fingers" are very rare. We note that the overall size (i.e., distance between tumor center and the farthest cell on tumor edge) of the tumors with distinct morphologies decrease as the ECM density and the associated pressure increase. Nonetheless, the emergence of finger-like structures significantly release the local pressure built up at the smooth surface of the growing tumor and thus, the growth of such invasion fingers is favored.

Figure 2 shows the snapshots of noninvasive tumors (e.g., $\gamma = 0$) growing in the random ECM with average initial density $\overline{\rho}^0_{\rm ECM} = 0.25, 0.45$ and 0.65, as well as the associated specific surface $s/(2/R_T)$ as a function of time. The ECM degradation ability value $\chi_0 = 0.2$ for the proliferative cells is used. Similar effects of the ECM density (i.e., pressure level) on the growth dynamics and tumor morphologies are observed, i.e., increasing the ECM density (pressure) leads to a continuous variation of tumor morphology ranging from smooth isotropic shapes to significantly fingered patterns. Since the heterogeneity of the ECM results in stronger local tumor surface roughness, the fingering effect is also stronger comparing with the corresponding homogeneous case with the same ECM density. In particular, the tumor growing in the ECM with $\overline{\rho}^0_{\rm ECM} = 0.65$ develops sub-fingers on the primary fingers, which is mainly caused by the local ECM density fluctuations (lower panel of Fig. 2). Such fine morphological features can hardly be resolved by continuum simulation method. The stronger fingering of tumors growing in the random ECM also leads to larger overall extents of the tumors.

B. Invasive Growth with Individual Cells Migrating into Surround ECM

Figure 3 shows the snapshots of invasive tumors growing in a homogeneous ECM with initial density $\rho^0_{\rm ECM} = 0.25, 0.45$ and 0.65 on day 120. Specifically, individual invasive cells can detach themselves from the primary tumor and migrate into the surrounding ECM. The following values of invasiveness parameters are used: mutation rate $\gamma = 0.05$, ECM

degradation ability value for the proliferative cells $\chi_0 = 0.25$, ECM degradation ability value for the invasive cells $\chi_1 = 0.75$, motility of the invasive cells $\mu = 4$, which corresponds to a high degree of malignancy.

It is clear from Fig. 3 that the tumor growing in the low-density ECM (e.g., under low pressure) ($\rho_{\rm ECM} = 0.25$) develops relatively short invasive branches (Fig. 3a), while the tumor growing in the high-density ECM (e.g., under high pressure) ($\rho_{\rm ECM} = 0.65$) possesses very long invasive branches (Fig. 3c). Also, we note that a large number of invasive cells are generated at the finger tips of the primary tumor, which in turns promotes the growth of the fingers. Since the invasive cells degrade the ECM close to the tumor surface, the local pressure exerted on the tumor is reduced. Thus, the degree of "fingering" in the invasive tumors is smaller than in the noninvasive ones. The invasive cells also enhance the growth of the primary tumor. Moreover, it can be seen that high ECM density (i.e., high pressure exerted on the tumor) enhances both fingering of the primary tumor and malignant behavior of invasive cells (Fig. 3c). We note that such invasion-tumor couplings have been extensively explored in Ref. 30.

Figure 4 shows the snapshots of invasive tumors growing in the random ECM with average initial density $\overline{\rho}^0_{\rm ECM} = 0.25, 0.45$ and 0.65 on day 120. The same values of invasiveness parameters as the homogeneous case are used. Again, the growth dynamics and tumor morphologies are qualitatively the same as the corresponding homogeneous case. However, the heterogeneity of the ECM enhances local tumor instability and thus, promotes the malignant behavior of the invasive tumor.

IV. CONCLUSIONS AND DISCUSSION

We have generalized a recently developed cellular automaton model to study the effects of pressure on the dynamics and tumor morphologies for both noninvasive proliferative growth and invasive growth with individual malignant cells detaching themselves from the primary tumor. In particular, we have explicitly taken into account the deformation of the extracellular matrix surrounding the tumor, which in turn imposes pressure on the neoplasm. Moreover, we also considered the local tumor-host interface instability, which can give rise to the emergence of finger-like protrusions of the tumor surface. We showed that by varying the ECM rigidity (i.e., the pressure level in the ECM), one can obtain a

variety of tumor morphologies ranging from spherical shapes to fingering patterns, which are quantitatively characterized by the specific surface. We also found that both high pressure and microenvironment heterogeneity can amplify the malignancy of the neoplasm in both the noninvasive proliferative case and the invasive case. Moreover, we demonstrated that the growth dynamics of the primary tumor and invasive cells are strongly coupled.

Figure 5 shows the morphology of ductal carcinoma *in situ* (DCIS), which resembles the morphology of noninvasive tumors growing in the ECM with intermediate density (Fig. 1(b) and Fig. 2(b)) predicted by our CA model. Strong fingering growth is rarely observed for DCIS, manly because the neoplasm is further constrained by a tight basal membrane composed of epithelial cells. Such complex microenvironment heterogeneities need to be incorporated in the CA model to accurately predict DCIS progression. On the other hand, significant fingering has been observed *in vitro*.[19] These experimental observations clearly demonstrate the robustness and predictive capability of our CA model.

We have shown that a high pressure in the ECM, which is due to large ECM density and deformation, can lead to significant fingering growth and enhance the malignant behavior of both the primary tumor and invasive cells. As a tumor grows in a confined microenvironment, it is inevitable that a high pressure will be built up. Thus, a tumor with a low level of malignancy initially can eventually develop highly malignant invasive behavior. Specifically, when finger-like protrusions develop, cells close to the finger tip have less contacting neighbors and thus, less adhesion. This makes it very easy for the invasive cells to leave the primary tumor and migrate deeply into the surrounding microenvironment, which ultimately leads to cancer metastasis.

Moreover, our results concerning the diversity of tumor morphologies enable one to infer the possible mechanisms behind the resulting shapes. For example, a noninvasive proliferative tumor possesses a morphology with significant finger-like protrusions on the tumor surface could be attributed to a host microenvironment in which the tumor grew that was very rigid and inhomogeneous. On the other hand, if such a tumor has a smooth and almost isotropic shape, it could mean that its host environment was very soft and homogeneous. For an invasive tumor with individual invasive cells that detach themselves from the primary tumor and migrate into the surrounding microenvironment, a rougher tumor surface could imply that the individual invasive cells possessed a strong ECM degradation ability, high motility and weak cell-cell adhesion.

Although our CA model is readily applied to model *in vitro* tumor growth, the heterogeneous microenvironments considered in the current model are highly idealized and do not include heterogeneities such as blood vessels and lymphatics, which could play an important role in clinical cancers. Incorporating more realistic microenvironments as well as other possible mechanisms (e.g., tumor and normal cell phenotypic plasticity and immune response) would lead to an improved model that could provide insights into *in vivo* tumor growth. Nonetheless, we expect that the conclusions drawn here still qualitatively apply to *in vivo* situations. Therefore, information on the tumor morphology, which can be obtained from histological images, is expected to lead to more accurate diagnosis and thus, more effective tumor treatment strategies. For example, if a tumor with a rough surface is detected, drugs that can release the high concomitant pressure in the host environment by modifying the molecular compositions of the ECM macromolecules could be used to reduce the malignancy of the tumor, leading to a noninvasive smooth isotropic shape. This not only could improve the efficiency of chemotherapy but also could make it easier to remove the tumor by resection. Finally, we note that improving the deliverability of chemotherapy will require application of existing theories to predict the transport properties of the underlying heterogeneous media.[39]

Acknowledgments

The research described was supported by the National Cancer Institute under Award NO. U54CA143803. The content is solely the responsibility of the authors and does not necessarily represent the official views of the National Cancer Institute or the National Institutes of Health.

---

* Electronic address: yjiao@princeton.edu

† Electronic address: torquato@electron.princeton.edu

[1] D. S. Coffey DS, *Nat. Med.* **4**, 882 (1998).

[2] D. Hanahan and R. A. Weinberg, *Cell* **100**, 57 (2000).

[3] T. S. Deisboeck, M. E. Berens, A. R. Kansal, S. Torquato, A. Rachamimov, D. N. Louis and E. A. Chiocca, *Cell Proliferat.* **34**, 115 (2001).

[4] I. J. Fidler, *Nat. Rev. Cancer.* **3**, 435 (2003).

[5] A. R. A. Anderson and M. A. J. Chaplain, *Bull. Math. Biol.* **60**, 857 (1998).

[6] J. L. Gevertz and S. Torquato, *J. Theor. Biol.* **243**, 517 (2006).

[7] J. L. Gevertz, G. T. Gillies and S. Torquato, *Phys. Biol.* **5**, 036010 (2008).

[8] J. L. Gevertz and S. Torquato, *Phys. Rev. E* **80**, 051910 (2009).

[9] A. R. A. Anderson, *Math. Med. Biol.* **22**, 163 (2005).

[10] A. R. A. Anderson, A. M. Weaver, P. T. Cummings and V. Quaranta, *Cell* **127**, 905 (2005).

[11] R. A. Gatenby and E. T. Gawlinski, *Cancer Res.* **56**, 5745 (1996).

[12] R. A. Gatenby, E. T. Gawlinski, A. F. Gmitro, B. Kaylor and R. J. Gillies, *Cancer Res.* **66**, 5216 (2006).

[13] H. B. Frieboes, X. M. Zheng, C. H. Sun, B. Tromberg, R. Gatenby and V. Gristini, *Cancer Res.* **66**, 1597 (2006).

[14] N. Bellomo and L. Preziosi, *Math. Comput. Model.* **32**, 413 (2000).

[15] M. Scalerandi, B. C. Sansone and C. A. Condat, *Phys. Rev. E* **65**, 011902 (2001.

[16] M. Scalerandi and B. C. Sansone, *Phys. Rev. Lett.* **89**, 218101 (2002).

[17] Y. Kim and A. Friedman, *Bull. Math. Biol.* **72**, 1029 (2010).

[18] A. M. Stein, T. Demuth, D. Mobley and M. Berens, *Biophys. J.* **92**, 356 (2007).

[19] P. Macklin and J. Lowengrub, *J. Thero. Biol.* **245**, 677 (2007).

[20] Y. Jiao and S. Torquato, *PLoS One* **6**, e27323 (2011).

[21] G. Helmlinger, P. A. Netti, H. C. Lichtenbeld, R. J. Melder and R. K. Jain, *Nature Biotech.* **15**, 778 (1997).

[22] M. C. Hogan, A. Lee, L. A. Solberg and S. D. Thome, *Am. J. Hematol.* **70**, 55 (2002)

[23] T. P. Padera, A. Kadambi, E. di Tomaso, C. M. Carreira, E. B. Brown, Y. Boucher, N. C. Choi, D. Mathisen, J. Wain, E. J. Mark, L. L. Munn and R. K. Jain, *Science* **296**. 1883 (2002).

[24] A. Bru and D. Casero, *J. Thero. Biol.* **243**, 171 (2006).

[25] M. J. Paszek, N. Zahir, K. R. Johnson, J. N. Lakins, G. I. Rozenberg, A. Gefen, C. A. Reinhart-King, S. S. Margulies, M. Dembo, D. Boettiger, D. A. Hammer and V. M. Weaver, *Cancer. Cell* **8**, 241 (2005).

[26] C. Guiot, P. Nicola, P. P. Delsanto and T. S. Deisboeck, *Phys. Biol.* **4**, P1 (2007).

[27] D. L. McElwain and G. J. Pettet, *Bull. Math. Biol.* **55**, 655 (1993).

[28] C. Y. Chen, H. M. Byrne and J. R. King, *J. Math. Biol.* **43**, 191 (2001).

[29] T. Roose, P.A. Netti, L.L. Munn, Y. Boucher and R.K. Jain, *Microvascular Res.* **66**, 204 (2003).

[30] Y. Jiao and S. Torquato, *PLoS Comput. Biol.* **7**, e1002314 (2011).

[31] S. Torquato, *Phys. Biol.* **8**, 015017 (2011).

[32] S. Torquato, *Random Heterogeneous Materials: Microstructure and Macroscopic Properties.* (Springer-Verlag, New York, 2002).

[33] A. R. Kansal, S. Torquato, G. R. Harsh, E. A. Chiocca and T. S. Deisboeck, *J. Theor. Biol.* **203**, 367 (2000).

[34] A. R. Kansal, S. Torquato, E. A. Chiocca and T. S. Deisboeck, *J. Theor. Biol.* **207**, 431 (2000).

[35] J. E. Schmitz, A. R. Kansal and S. Torquato, *J. Theor. Med.* **4**, 223 (2002).

[36] L. A. Liotta, C. N. Rao and S. H. Barsky, *Lab. Invest.* **49**, 636 (1983).

[37] M. Sarntinoranont, F. Rooney and M. Ferrari, *Annals of Biomedical Engineering* **31**, 327 (2003).

[38] V. D. Gordon, M. T. Valentine, M. L. Gardel, D. Andor-Ardo, S. Dennison, A. A. Bogdanov, D. A. Weitz and T. S. Deisboeck, *Experimental Cell Res.* **289**, 58 (2003).

[39] S. Torquato, *J. Chem. Phys.* **84**, 6345 (1986); J. Rubinstein and S. Torquato, *J. Fluid Mech.* **206**, 25 (1989); S. Torquato and A. K. Sen, *J. Appl. Phys.* **67**, 1145 (1990); S. Torquato, *Phys. Rev. Lett.* **64**, 2644 (1990); S. Torquato and M. Avellaneda, *J. Chem. Phys.* **95**, 6477 (1991).

FIG. 1: Upper panel: Snapshots of a noninvasive tumor growing in homogeneous ECM with density $\rho_{\rm ECM} = 0.25$ on day 40 (a1), day 80 (a2) and day 120 (a3) after initialization. The associated specific surface $s/(2/R_T)$ (a4) remains small in value as the tumor grows, indicating a compact tumor morphology. Middle panel: Snapshots of a noninvasive tumor growing in homogeneous ECM with density $\rho_{\rm ECM} = 0.45$ on day 40 (b1), day 80 (b2) and day 120 (b3) after initialization. The associated specific surface $s/(2/R_T)$ (b4) shows a rapid growth after day 100, indicating fingering growth of the tumor. Lower panel: Snapshots of a noninvasive tumor growing in homogeneous ECM with density $\rho_{\rm ECM} = 0.65$ on day 40 (c1), day 80 (c2) and day 120 (c3) after initialization. The associated specific surface $s/(2/R_T)$ (c4) increase monotonically as the tumor grows, indicating significant fingering of the tumor.

FIG. 2: Upper panel: Snapshots of a noninvasive tumor growing in random ECM with average density $\overline{\rho}_{\rm ECM} = 0.25$ on day 40 (a1), day 80 (a2) and day 120 (a3) after initialization. The associated specific surface $s/(2/R_T)$ (a4) remains small in value as the tumor grows, indicating a compact tumor morphology. Middle panel: Snapshots of a noninvasive tumor growing in random ECM with average density $\overline{\rho}_{\rm ECM} = 0.45$ on day 40 (b1), day 80 (b2) and day 120 (b3) after initialization. The associated specific surface $s/(2/R_T)$ (b4) shows a rapid growth after day 100, indicating fingering growth of the tumor. Lower panel: Snapshots of a noninvasive tumor growing in random ECM with average density $\rho_{\rm ECM} = 0.65$ on day 40 (c1), day 80 (c2) and day 120 (c3) after initialization. The associated specific surface $s/(2/R_T)$ (c4) increase monotonically as the tumor grows, indicating significant fingering of the tumor. Note that sub-fingers are developed on the primary fingers.

FIG. 3: Snapshots of invasive tumors growing in a homogeneous ECM with different densities on day 100. Individual invasive cells detach themselves from the primary tumor, locally degrade the ECM and migrate into the surrounding microenvironment. (a) $\rho_{\rm ECM} = 0.25$ (b) $\rho_{\rm ECM} = 0.45$ (c) $\rho_{\rm ECM} = 0.65$. Note that the tumor growing in the low-density ECM (pressure) ($\rho_{\rm ECM} = 0.25$) develops relative short invasive branches [see panel (a)], while the tumor growing in the high-density ECM (pressure) ($\rho_{\rm ECM} = 0.65$) possesses very long invasive branches [see panel (c)].

FIG. 4: Snapshots of invasive tumors growing in a random ECM with different average densities on day 100. Individual invasive cells detach themselves from the primary tumor, locally degrade the ECM and migrate into the surrounding microenvironment. (a) $\overline{\rho}_{\rm ECM} = 0.25$ (b) $\overline{\rho}_{\rm ECM} = 0.45$ (c) $\overline{\rho}_{\rm ECM} = 0.65$. Note that the tumor growing in the low-density ECM (pressure) ($\rho_{\rm ECM} = 0.25$) develops relative short invasive branches [see panel (a)], while the tumor growing in the high-density ECM (pressure) ($\rho_{\rm ECM} = 0.65$) possesses very long invasive branches [see panel (c)]. Also observe that invasive cells clump at the finger tips of the primary tumor, which in turns promotes the growth of the fingers [see panel (c)].

FIG. 5: An image showing the morphology of ductal carcinoma in situ with bumpy surface. Image courtesy of R. Gatenby.

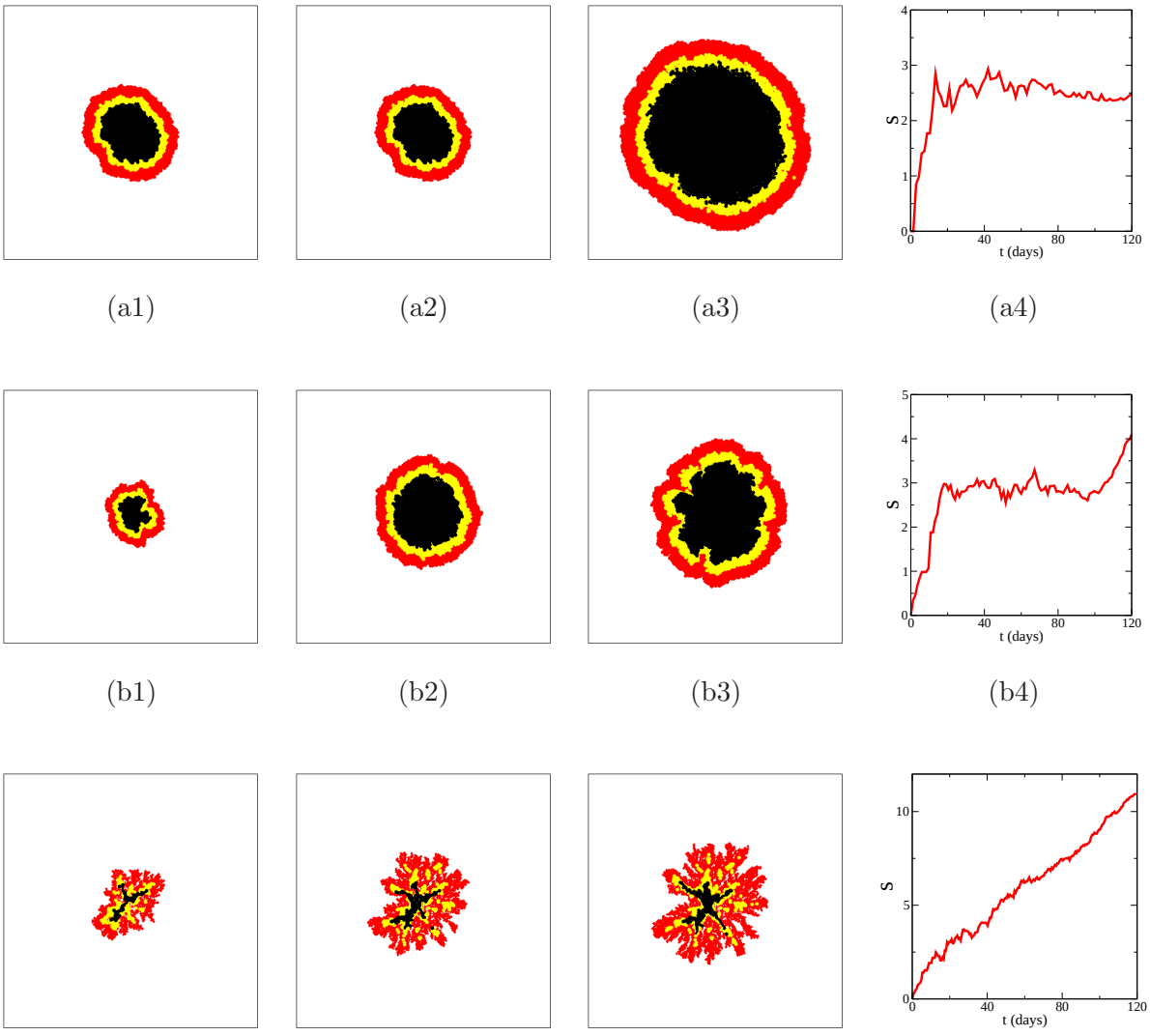

(a1) (a2) (a3) (a4)

(b1) (b2) (b3) (b4)

(c1) (c2) (c3) (c4)

FIG. 1: Jiao, Torquato

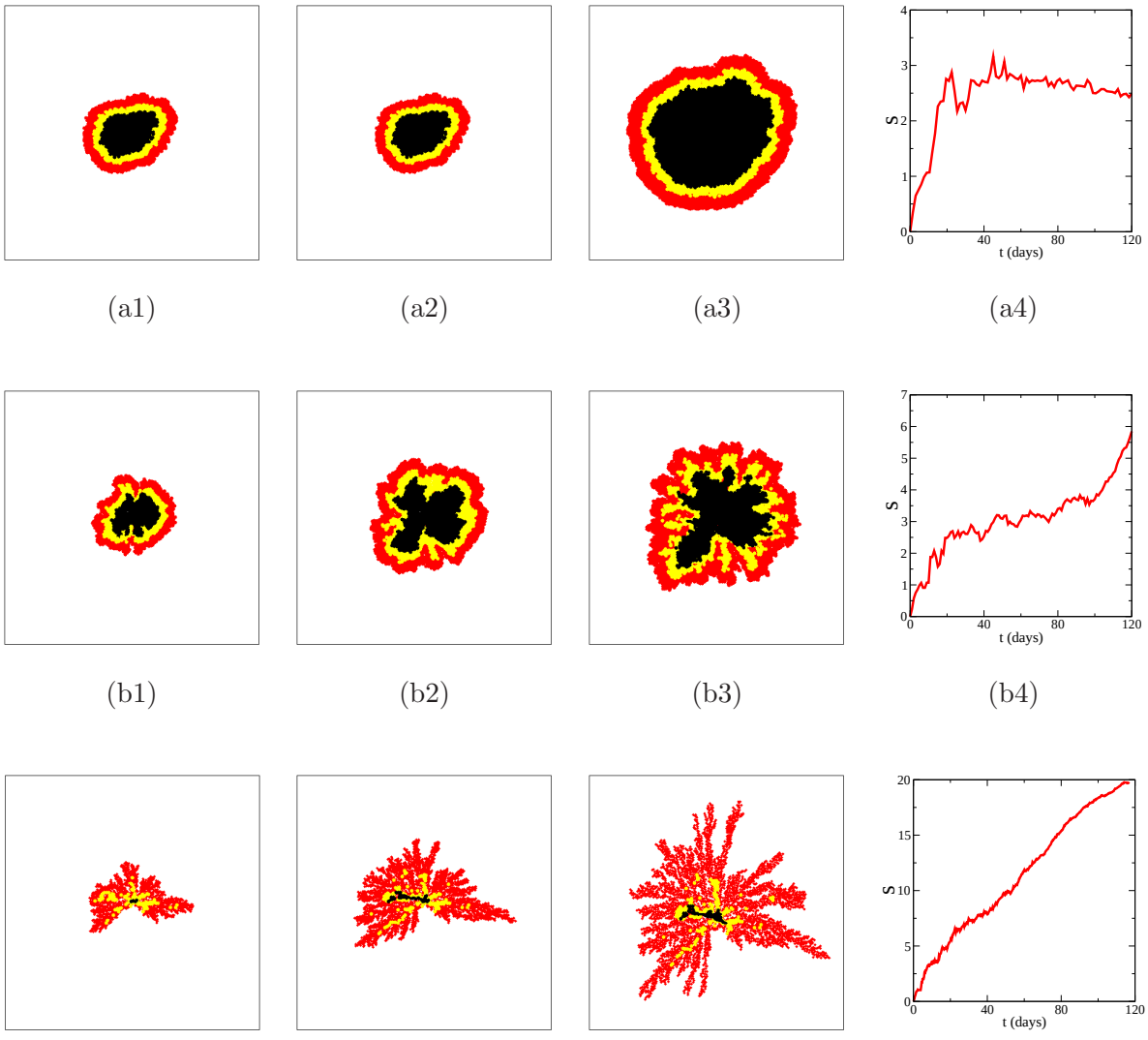

(a1) (a2) (a3) (a4)

(b1) (b2) (b3) (b4)

(c1) (c2) (c3) (c4)

FIG. 2: Jiao, Torquato

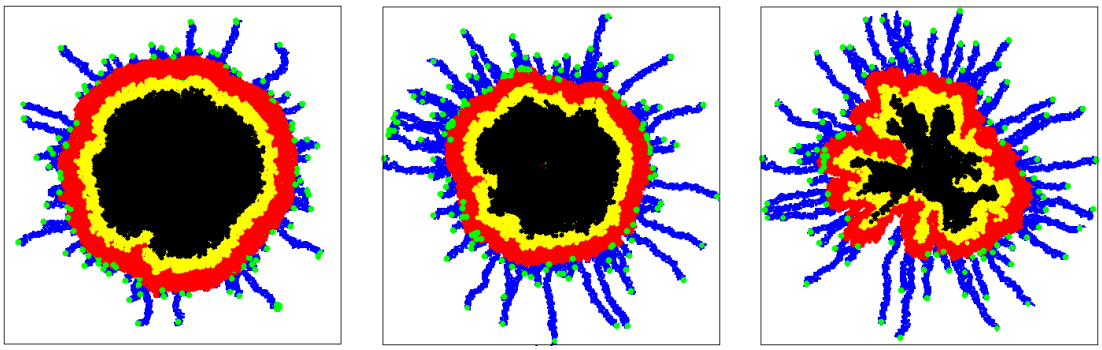

(a) (b) (c)

FIG. 3: Jiao, Torquato

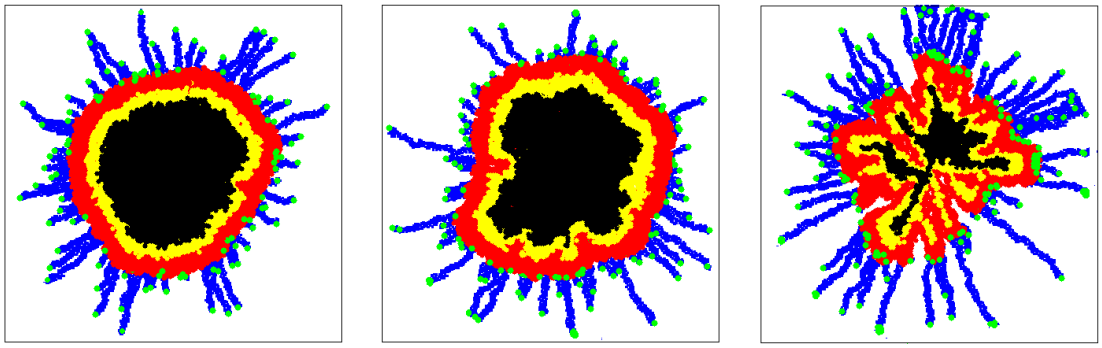

(a) (b) (c)

FIG. 4: Jiao, Torquato

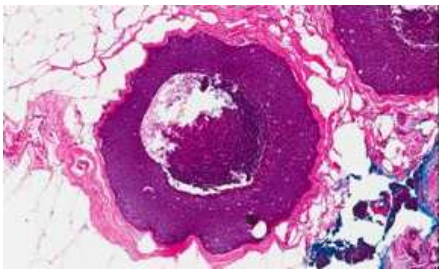

FIG. 5: Jiao, Torquato